

Daily INSOLation (DINSOL-v1.0): an intuitive tool for classrooms and specifying solar radiation boundary conditions

Emerson Damasceno Oliveira

Laboratory of Meteorology, Federal University of Vale do São Francisco (UNIVASF), 48902-300, Juazeiro-BA, Brazil

Correspondence: Emerson D. Oliveira (emerson.oliveira@univasf.edu.br)

Abstract. Climate modelling requires spending an extensive amount of time programming, which means reading, learning, testing, and evaluating source code. Fortunately, many climate models have been developed within the past decades, making it easier for climate studies to be conducted on a global scale. However, some climate models have millions of code lines, making the introduction of new parameterizations a laborious task that demands teamwork. While it is true that the high-complexity models perform realistic climate simulations, some researchers perform their studies using simplified climate models in the preliminary test phases. This realisation motivated the development of the Daily INSOLation (DINSOL-v1.0), a robust computer program to support the simplified climate models, performing solar radiation calculations while considering Milankovitch cycles and offering various simulation options for its users. DINSOL was intended to function as a program that supplies data (e.g., daily insolation, instantaneous solar radiation, orbital parameters of the Earth, and calendar dates), such as the PMIP. While preparing the boundary conditions of solar radiation for climate models, it was realised that the DINSOL model could also be a helpful tool for use in classrooms. Thus, it was decided that an intuitive graphical user interface would be required to cater to this educational purpose. The model was written in the Fortran 90 language, while its graphical user interface would be built using PyGTK, a Python application programming interface (API) based on GIMP ToolKit (GTK). Furthermore, the R language would also be used to generate a panel containing contour fields and sketches of the orbital parameters to support the graphical execution. The model evaluation made use of data from PMIP and other tools, and the data analysis was performed through statistical methods. Once all tests were concluded, an insignificant difference between the DINSOL-obtained results and the results obtained from other models validated the viability of DINSOL as a dependable tool.

1 Introduction

In paleoclimatology, greenhouse gases (GHGs) and other climate features, such as air temperature, can be estimated using indirect methods (e.g., ice cores, speleothems, tree rings, lake and marine sediments, glacier fluctuations, and others) (Klippel et al., 2020). Paleoclimatology also investigates the effect that changes in the orbit of the Earth has on the incoming solar radiation (ISR). GHGs are vital because they affect the net radiation by increasing or decreasing the heat trapped in the atmosphere. Therefore, fluctuations in ISR or GHG affect the global energy balance, meaning that they are factors in global climate change (Menviel et al., 2019; Lhardy et al., 2021). Berger (2021) details how a century ago, Milutin Milankovitch proposed a revolutionary approach to explaining the quasi-periodic occurrence of ice-ages from caloric season measurements.

It was because of his contributions that he has been considered as the father of paleoclimate modelling. Thus, the conceptual climate model developed and adopted by Milankovitch assumed that ISR changes happened due to cyclic oscillations of the Earth's Orbital Parameters (EOP): obliquity, eccentricity, and precession of the equinox. From Puetz et al. (2016), the initial Milankovitch theory was treated with scepticism due to previous theories on what causes ice-ages, theories relating to the ejection of volcanic dust content in the atmosphere, as well as the cyclic changes in the magnetic field of the Earth.

Berger (2021) states that the most important books published by Milankovitch are *Théorie mathématique* (1920) and *Kanon der Erdbestrahlung* (1941). In these books and other literature, Milankovitch used EOP data previously calculated, adopting Stockwell–Pilgrim values from the theoretical investigations on ISR and ice-ages. From Crucifix et al. (2009), besides Milankovitch; other authors investigated the relationship between ice-ages and ISR, the most distinguished being André Berger, who developed a practical method to calculate the EOP from trigonometric series. He also adopts the caloric seasons to investigate the past climate as a function of the EOP. In the 1970s, Berger published papers (e.g., Berger, 1976, 1977, 1978a, b) that consolidated the modern concepts of ISR modelling. Since then, novel solutions for Earth's orbit cycles have been developed (e.g., Laskar, 1988; Berger and Loutre, 1991; Laskar et al., 1993, 2004, 2011).

Presently, the Paleoclimate Modelling Intercomparison Project (PMIP) represents the best efforts of the scientific community in paleoclimate reconstructions. PMIP is in its fourth phase (PMIP4), with some studies ongoing and others already been published (e.g., Jungclaus et al., 2017; Otto-Bliesner et al., 2017; Kageyama et al., 2018; Menviel et al., 2019). For instance, second Brierley et al. (2020), PMIP simulations suggest that during the mid-Holocene, the most pronounced and robust monsoonal changes occurred over northern Africa and the Indian subcontinent, where the simulated rain rate was 10% greater than the pre-industrial era (1850 CE). Therefore, climate reconstructions are crucial to enhancing the hold on understanding of natural forcings. Moreover, the Coupled Model Intercomparison Project (CMIP) is capable of handling various scenarios, considering natural and anthropogenic forcings, and reducing the uncertainties of climate projections (Eyring et al., 2016). Further, the Intergovernmental Panel on Climate Change (IPCC) is responsible for announcing the CMIP scenarios through assessment reports, focusing mainly on providing readable summaries for policymakers (Fischer et al., 2020).

In recent years, useful tools to aid in calculating the EOP and insolation were developed, tools like the PALINSOL, an R package written by Michel Crucifix that adopts Berger (1978b), Berger and Loutre (1991), and Laskar et al. (2004) solutions. Another tool is the Earth-Orbit v2.1, a MATLAB program created by Kostadinov and Gilb (2014) to calculate the EOP according to the Berger (1978b) and Laskar et al. (2004) methodologies. The PALINSOL and other similar Fortran programs written by André Berger are available to download by the Université Catholique de Louvain (UCLouvain) through the Earth and Life Institute web page (<https://www.elic.ucl.ac.be/modx/index.php?id=83>, last access: 21 January 2023).

Even though we have pre-existing programs to calculate the ISR following the Milankovitch cycles theory, they were developed to cater to different purposes and kinds of users. For instance, the PALINSOL package assumes that users already know to program in R language, which could be an obstacle for students at the beginner level. Thus, the Earth-Orbit v2.1 could be an alternative to get around the programming skills requirement once it can be executed using a friendly GUI. Even still, it is expected that the Earth-Orbit v2.1 users buy a MATLAB license, which could be prohibitive to disadvantaged groups.

Furthermore, none of these programs were idealized to be executed from only one command line or clique and, from that, prepare the boundary conditions of simplified climate models. Therefore, it would be helpful to have another software option that works similarly to the pre-existent tools but, additionally, should be free and does not require any programming language skills to execute simple tasks, such as computing the daily insolation globally for a given year.

65 To achieve this goal, the Daily INSOLation (DINSOL-v1.0) program was developed, intended to be an intuitive and versatile tool ideal for paleoclimate simulations, such as those performed on the PMIP, and still helpful for education purposes. From DINSOL, users can prepare solar radiation as a boundary condition for simplified climate models quickly and flexibly. Moreover, the DINSOL source code brings many comments, allowing advanced users to modify and adapt it more intuitively than other tools. For instance, introducing a new calendar option to compute the annual daily insolation for an exoplanet is a
70 simple deployment. Still, a standard execution offers for users various input choices to run their DINSOL simulations (e.g., year, solar constant, calendar, latitudinal and longitudinal number points). It also includes a graphical user interface (GUI), with the GUI written in PyGTK, a Python program that adopts the GTK library. Basically, the DINSOL source code is mostly a Fortran program because all its important processes (e.g., data reading, taking decisions, calculation, and writing results) were written using Fortran 90 language. Besides PyGTK and Fortran 90, the model also contains some script templates written
75 in R language to assist its users in accessing computed solar radiation data. The program has a GNU GPL-v3.0 license, which allows users to modify, share, and improve it. For instance, the DINSOL was adapted to prepare ISR data for an energy balance model used by Oliveira and Fernandez (2020).

Ultimately, the following chapters describe the program source code, giving a detailed explanation of the astronomical equations, ISR and EOP parameterizations, input and output data, as well as a model evaluation chapter, where we adopted the
80 PMIP and other data sources as a reference.

2 Astronomical aspects and model description

This section details the astronomical fundamentals required to understand the DINSOL source code. The variables, constants, and mathematical relations are explained in the subsequent subchapters.

2.1 Main orbital elements and some formulas

85 The DINSOL model utilises heliocentric coordinates, such as in Berger (1978b) and Berger et al. (2010), and the most important information on the Earth's orbit is shown in Figure 1. From the first figure, we have some orbital elements and constants for the modern days:

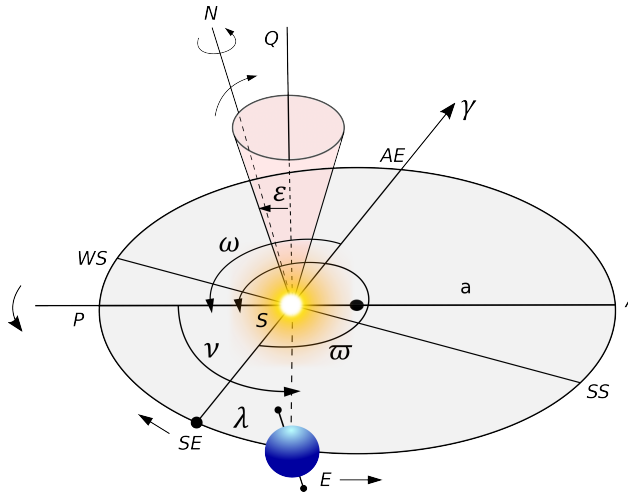


Figure 1. Heliocentric coordinates sketch based in Berger (1978b) and Berger et al. (2010). The orbital elements are denominated of Earth, E , Sun, S , the semi-major axis of the Earth's orbit, a , perihelion, P , aphelion, A , vernal point, γ , spring equinox, SE , summer solstice, SS , autumn equinox, AE , winter solstice, WS , longitude of the perihelion, ϖ , longitude of the perigee, ω , true solar longitude, λ , true anomaly, ν , obliquity, ε . The SQ is perpendicular to the ecliptic, and N is the north pole.

$$S_0 = 1366 \text{ W/m}^2$$

90 $T = 365.2422 \text{ days/year}$

$$a \sim 150 \times 10^6 \text{ km}$$

$$e = 0.016724$$

$$\varepsilon = 23.446^\circ$$

$$\varpi = 282.04^\circ$$

95 $\omega = 102.04^\circ$

where the solar constant, S_0 , the tropical year, T , the semi-major axis, a , and eccentricity of the Earth's elliptical orbit, e . The longitude of the perihelion is kept unchanged, ϖ , given from vernal point (March 21) until perihelion day, and the longitude of the perigee, ω , that is ϖ added to 180° . As shown in Figure 1, the Earth's orbital revolution occurs counterclockwise, while the equinoxes precession occurs clockwise.

100 Regarding Figure 1, the Earth's obliquity representing the equatorial plane, ε , given by a perpendicular cone to the ecliptic plane, the Earth-Sun distance, r , measured in units of the semi-major axis, a , been given by the ellipse equation:

$$\rho = \frac{r}{a} = \frac{1 - e^2}{1 + e \cos \nu} \quad (1)$$

where the relative Earth-Sun distance, ρ , provides values for an annual calendar, such as the Figure 2. The true anomaly, ν , is measured counterclockwise from the perihelion and given by the equation $\nu = \lambda - \varpi$, where λ represents the true solar longitude. Equation 1 is given in Beutler (2005, p. 127).

The DINSOL model implements the methodology from Berger (1978b), which solves λ in a few steps assuming that the start day is the vernal equinox (March 21), where $\lambda = 0$. Thus, we first need to find the mean longitude λ_m , however, before is necessary to calculate the λ_{m0} using the equation 2, where $\beta = \sqrt{1+e^2}$ and e is the eccentricity.

$$\lambda_{m0} = \lambda - 2 \left[\left(\frac{1}{2}e + \frac{1}{8}e^3 \right) (1 + \beta) \sin(\lambda - \varpi) - \frac{1}{4}e^2 \left(\frac{1}{2} + \beta \right) \sin 2(\lambda - \varpi) + \frac{1}{8}e^3 \left(\frac{1}{3} + \beta \right) \sin 3(\lambda - \varpi) \right] \quad (2)$$

Finally, λ is calculated using equation 3, implementing a loop that solves λ along one year. However, for the first day (first iteration), the model requires λ_{m0} value obtained previously from equation 2 where we assume $\lambda_m = \lambda_{m0}$, to be employed. Hence, in the proceeding days, λ_m must be calculated from a simple increment equation given by the formula $\lambda_{m(i)} = \lambda_{m(i-1)} + 360/N_d$, where N_d represents the number of days within one year. In the DINSOL, two annual calendars are available, a 365-day and 360-day calendar.

$$\lambda = \lambda_m + \left(2e - \frac{1}{4}e^3 \right) \sin(\lambda_m - \varpi) + \frac{5}{4}e^2 \sin 2(\lambda_m - \varpi) + \frac{13}{12}e^3 \sin 3(\lambda_m - \varpi) \quad (3)$$

Figure 2 represents the annual variation of Earth-Sun distance, ρ , for the present day. Furthermore, the data used to plot ρ was simulated using DINSOL, solving equations 1 to 3. A calendar conversion was initialised with a starting date of January 1st instead of March 21. The subsequent chapter contains all the details of the calendar conversions in the source code.

2.2 Defining the calendar dates

The daily insolation algorithm used in Berger (1978b) uses classical astronomical equations where the year is initialised from spring equinoxes, like the solar Hijri calendar, also known as the Persian or Iranian calendar. The Persian calendar accurately calculates the length of a season due to the use of the true solar longitude, λ , which works on elliptical coordinates, like in Kepler's laws. Although Berger (1978b) assumed March 21 as the fixed date for spring equinoxes, season dates oscillate over the years. For instance, in Borkowski (1996), in the second half of the 21st century, the spring equinoxes will occur on March 19 and 20 dates. An online program offered by NASA can accurately calculate the date of astronomical events using the Gregorian calendar (<https://data.giss.nasa.gov/modelE/ar5plots/srvernal.html>, last access: 21 January 2023). The Gregorian calendar is lunisolar and assumes the temporal definition of months and seasons, where the astronomical dates change slowly (Joussaume and Braconnot, 1997). For instance, considering λ , the assumption is that seasons stay at 90° from one another along an elliptical orbit. Furthermore, a common challenge for paleoclimate simulations is the comparison of past and present climates, considering the differences between calendars.

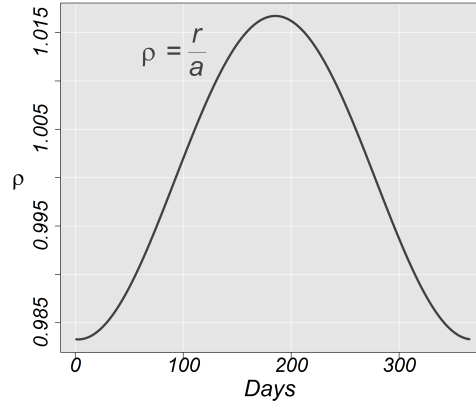


Figure 2. Relative Earth-Sun distance, ρ , along one year in Astronomical Unit (AU) for current days.

From Bartlein and Shafer (2019), the number of days in a month are not constant, which means that the first day of each month might occur in a different position relative to the current Gregorian calendar. For instance, in Joussaume and Braconnot (1997), during the Eemian periods, the January month should have 34 days and start on December 25 compared to our current calendar. PMIP assumes the vernal equinox as the time reference, keeping the current format of the Gregorian calendar for any period, which allows variations in seasons length, as well as changes in the aphelion and perihelion dates. From this method, the models can compare the results of paleoclimate simulations by using the same calendar structure, assuming a standard format. A typical PMIP experiment assumes a 365-day calendar, while intermediate-complexity climate models commonly work with a 360-day calendar.

The astronomical event dates (seasons, perigee, and apogee) are functions of the changes in two orbital parameters: eccentricity and precession of equinoxes. Furthermore, it must be noted that DINSOL supports a 365-day and 360-day calendar. Consequently, it must be considered that the vernal equinox (March 21) always occurs on the 80th day of a 365-day calendar and on the 81st day of a 360-day calendar. Thus, a modified version of equation 2 must be implemented assuming a simple calendar conversion (solar to Gregorian calendar), where estimation of the perihelion and aphelion dates will be made using the equation 4.

$$\begin{aligned}
 P_d = -\varpi - 2 & \left[\left(\frac{1}{2}e + \frac{1}{8}e^3 \right) (1 + \beta) \sin(-\varpi) \right. \\
 & - \frac{1}{4}e^2 \left(\frac{1}{2} + \beta \right) \sin 2(-\varpi) \\
 & \left. + \frac{1}{8}e^3 \left(\frac{1}{3} + \beta \right) \sin 3(-\varpi) \right] \quad (4)
 \end{aligned}$$

where P_d represents the perihelion day on a solar calendar, and P_d can be converted for a day in the Gregorian calendar if equation 5 is used. The assumption that the vernal point (March 21) is called M_{21} , which accepts the values 80 or 81 in

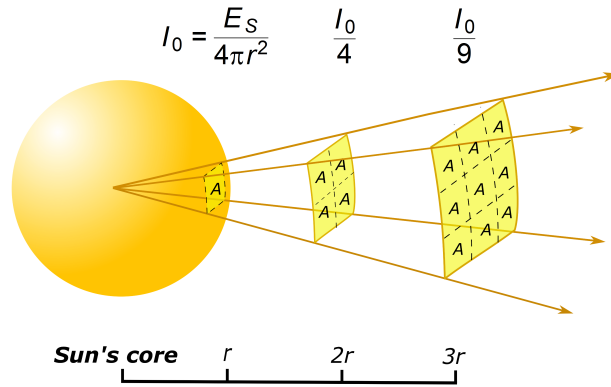


Figure 3. Sketch of the solar flux density (I_0) as a function of the distance to the Sun's core.

concordance with the chosen calendar, $N_d = 365$ or $N_d = 360$, respectively.

$$P_d = M_{21} + |P_d| \frac{N_d}{360} \quad (5)$$

After obtaining P_d for a day of the year in the Gregorian calendar, the aphelion day can be determined, A_d , adopting the equation 6:

$$155 \quad A_d = P_d + \frac{N_d}{2} \quad (6)$$

The DINSOL model has a subroutine that converts the day of the year to its correspondent month and day. Moreover, beyond perihelion and aphelion dates, the start date of a season can be determined. A fixed date for the spring equinox (March 21) must be assumed, $\lambda = 0^\circ$. Then, using the true solar longitude, λ , the Summer, Autumn, and Winter start dates are known, at $\lambda = 90^\circ$, $\lambda = 180^\circ$, and $\lambda = 270^\circ$, respectively. Hence, conform was discussed in section 2.1, λ must be solved using a loop to determine the iterations corresponding to λ equal to 90° , 180° , and 270° . Furthermore, the DINSOL model uses a two-decimal precision, like in the PMIP II project. The calendar function evaluation is provided in subchapter 3.2.

2.3 Modelling the solar irradiance on the top of the atmosphere

In Fu (2006, p. 116), the incoming solar radiation (ISR) on the top of the atmosphere, S_0 , is estimated by the solar flux density (I_0), which assumes an isotropic concentric emittance from the Sun. The total solar emittance, E_S , must be constant, regardless of the size of the sphere area. The flux density adheres to the inverse square law, meaning that energy per area must diminish when the distance from the energy source increases, as shown in Figure 3.

Therefore, E_S can be estimated doing the multiplication of the solar sphere area by their emission in a one-meter square, being the emission calculated using the Stefan-Boltzmann law, $E_b = \sigma T^4$, assuming the photosphere temperature and the solar radius as $T = 6000 \text{ K}$ and $r = 6.96 \times 10^8 \text{ m}$, respectively (Hartmann, 2016, p. 29). The flux density on the Earth's orbital

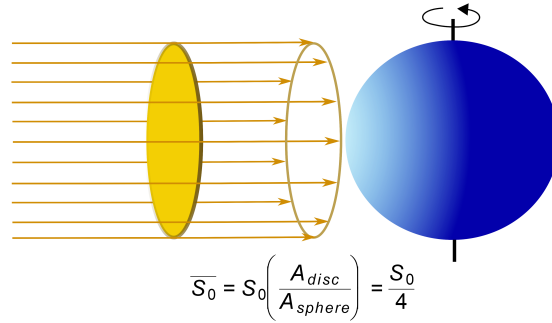


Figure 4. The incoming solar radiation as a parallel beam and its global average, \bar{S}_0 .

170 position, S_0 , can be estimated using a hypothetical solar sphere of radius $a = 150 \times 10^9 m$, the Earth-Sun distance. The solar constant is thus $S_0 \approx 1366 Wm^{-2}$.

During simplified climate analysis, the global ISR average is \bar{S}_0 , and because of the large Earth-Sun distance, the solar radiation is assumed to be a parallel and uniform beam Hartmann (2016, p. 31). Thus, to estimate \bar{S}_0 , the total ISR inside of the disc area, the cross-section, must be divided by the Earth sphere area (Figure 4), resulting in $\bar{S}_0 \approx 340 Wm^{-2}$.

175 Although simplified climate approaches on zero-dimensional models are viable in classrooms, complex climate investigations require providing a realistic ISR. This way, the DINSOL model implements two different methods to calculate the ISR in the outer atmosphere. The first method is *daily insolation* (Q_0) and the second is *instantaneous solar radiation* (Q_I). Thus, using this information, the methods can now be elaborated on.

1) Daily insolation

180 To calculate the ISR, aspects of ISR incidence on spherical surfaces must be considered (e.g., solar zenith angle (Z), hour angle (H), solar declination (δ), latitude (ϕ), and the relative Earth-Sun distance (ρ)). Thus, In Liou (2002, p. 51), a realistic model of the daily insolation can be generated using the equation 7:

$$Q_0 = S_0 \left(\frac{a}{r} \right)^2 \cos Z \quad (7)$$

185 where S_0 is the solar constant and $(a/r)^2$ represents the inverse square of the relative Earth-Sun distance, $1/\rho^2$. The steps to calculate ρ were listed section 2.1. The solar zenith angle, Z , is obtained from the spherical law of cosines, shown in the equation 8:

$$\cos Z = \sin \phi \sin \delta + \cos \phi \cos \delta \cos h \quad (8)$$

where h is the hour angle for a small time interval. To obtain the daily insolation, the total ISR at any latitude for a given day requires calculating daily ISR from sunrise (SR) to the sunset (SS).

$$190 \quad Q_0 = \int_{SR}^{SS} S_0 \left(\frac{a}{r} \right)^2 (\sin \phi \sin \delta + \cos \phi \cos \delta \cos h) dt \quad (9)$$

In equation 9 the constants for a given day are δ , ϕ and $(a/r)^2$. The hour angle and time are associated with the angular speed of Earth, Ω . Thus, a time differential substitution, dt , assuming $dt = dh/\Omega$, can be implemented. Result in equation 9 being a function of h :

$$Q_0 = \frac{S_0}{\Omega} \left(\frac{a}{r}\right)^2 \left[\sin \phi \sin \delta \int_{-H}^H dh + \cos \phi \cos \delta \int_{-H}^H \cos h dh \right] \quad (10)$$

195 where the hour angle between the sunrise until solar noon is $-H$ and from the solar noon until sunset is $+H$, then solving the integral yields equation:

$$Q_0 = \frac{2S_0}{\Omega} \left(\frac{a}{r}\right)^2 (H \sin \phi \sin \delta + \cos \phi \cos \delta \sin H) \quad (11)$$

Therefore, assuming that the angular speed of Earth is $\Omega = 2\pi/86400$, the equation for accumulated solar radiation in one day, that is, the daily insolation can be found. However, the DINSOL model provides the daily average of the ISR, which 200 requires the simplification of the equation by removing the total seconds per day. Finally, the equation implemented in the DINSOL source code:

$$Q_0 = \frac{S_0}{\pi} \left(\frac{a}{r}\right)^2 (H \sin \phi \sin \delta + \cos \phi \cos \delta \sin H) \quad (12)$$

Now, using Berger (1978b), to estimate Q_0 following the equation 12, it is necessary to calculate $\sin \delta$, $\cos \delta$, $\cos H$, $\sin H$, and H , requires the implementation of these equations:

$$205 \quad \sin \delta = \sin \varepsilon \sin \lambda \quad (13)$$

$$\cos \delta = \sqrt[2]{1 - \sin^2 \delta} \quad (14)$$

$$\cos H = -\tan \phi \tan \delta \quad (15)$$

where λ is the true solar longitude, already explained and ε is the Earth obliquity, $\cos H$ demands the initialisation of the following conditions:

$$210 \quad f(H) = \begin{cases} \cos H < -1, & \cos H = -1 \\ \cos H > 1, & \cos H = 1 \end{cases} \quad (16)$$

Finally, these are the last steps:

$$\sin H = \sqrt[2]{1 - \cos^2 H} \quad (17)$$

$$H = \arccos(\cos H) \quad (18)$$

Prior to the initialisation of the *instantaneous solar radiation* method, the equation used to calculate the day length, in terms 215 of number of hours of sunlight (N) is:

$$N = \frac{2H}{15} \quad (19)$$

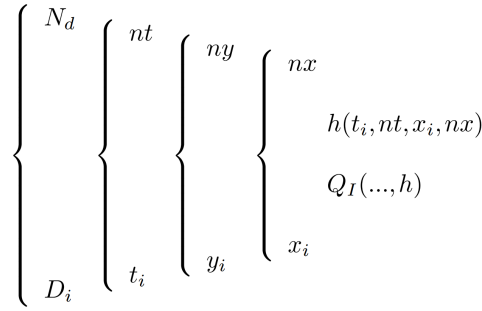


Figure 5. An example of the loop employed to run the instantaneous solar radiation subroutine.

2) Instantaneous solar radiation

The DINSOL model has a subroutine dedicated to calculating the instantaneous solar radiation, Q_I , this subroutine employs equations 7 and 8. The main difference between Q_I and Q_0 is that while Q_0 stores a single value per day, Q_I can store several values per day (hours or minutes). Another key difference is that Q_I is calculated globally, while Q_0 simulates only the latitudinal effect. Below is the equation 20 used to calculate Q_I :

$$Q_I = S_0 \left(\frac{a}{r}\right)^2 (\sin \phi \sin \delta + \cos \phi \cos \delta \cos h) \quad (20)$$

The equation 20 is calculated using four nested loops (Figure 5), where the first loop represents the passage of the days in a year, D_i , the second loop is the time interval, t_i , within one day (e.g., 6 h, 3 h, 1 h, etc.), such as is that shown in Figure 6. The third nested loop represents the latitudes, y_i , and finally, the fourth contains the longitudinal loop, x_i .

Following is given the hour angle, h , as a function of the time interval, t_i , and longitude x_i :

$$h = -\pi + \left(\frac{2\pi}{nt}\right)(t_i - 1) + \left(\frac{2\pi}{nx}\right)(x_i - 1) \quad (21)$$

Therefore, after calculating h , the results must be substituted into equation 20, where the other variables may be calculated using the Q_0 method, and negative Q_I values are assumed as zero. The algorithm for the hour angle initiates from the west in the eastwards direction, following the Earth's rotation about its axis. Thus, considering the first day, D_1 , and the first hour (0 UTC), t_1 , the hour angle must be calculated globally. This means that an hour angle covering all longitudinal points from the west to the east must be calculated for each latitude. This way, from the first timestep, t_1 , the algorithm starts the second timestep, t_2 , which is the same data calculated previously at t_1 , after a westward rotation (Figure 6). Hence, iterations must repeat for 24 h, before the start of the second day, D_2 , where changes in solar declination, δ , and Earth-Sun distance, ρ , must be considered. In summary, this subroutine is responsible for realistically simulating the ISR in the outer atmosphere to ensure that the program is viable for more complex deployments or studies that require accurate simulations of the effect of the day-to-night transition.

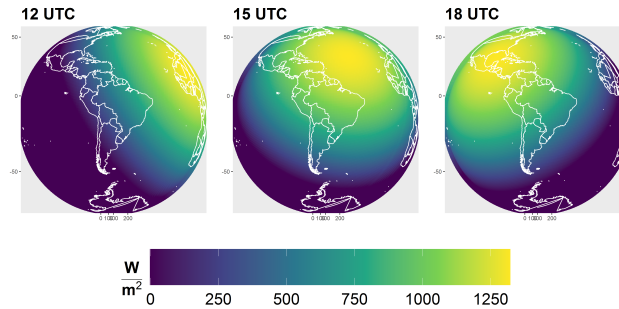


Figure 6. The instantaneous solar radiation on the top of the atmosphere from the DINSOL model for nowadays on June 29.

2.4 Orbital motions: parameterizations

The law of universal gravitation computes the mutual attraction force between two bodies and, according to Yang (2017), their
 240 formula is:

$$F = -G \frac{Mm}{a^2} \hat{r} \quad (22)$$

for the Sun-Earth case, M represents mass of the sun, m the mass of the earth, G is the universal gravitational constant, $G = 6.6739 \times 10^{-11} Nm^2/kg^2$, and \hat{r} is a unitary vector. The Earth-Sun distance, a , is given by the average radius of the Earth's orbit.

245 Although Newton adopted the gravitational law for two celestial bodies with success (e.g., Sun-Earth, Earth-Moon, Sun-Mars, etc), three-body problems proved to be more complex. Precise astronomical predictions require considering the gravitational influence of the other celestial bodies (Laskar et al., 2004). Euler and Lagrange found particular solutions for the three-body problem (Musielak and Quarles, 2017). In the late 1880s, Heinrich Bruns and Henri Poincaré showed that a general arrangement of three or more bodies (*n-body problem*) yielded no analytical solution (Hamilton, 2016).

250 Though complex astronomical motions cannot admit analytical solutions, a distinguished researcher overcame this obstacle by adopting the spectral decomposition technique. André Berger made it possible for anyone to estimate the Earth's orbital parameters (EOP) within ± 1 Myr of the present (Crucifix et al., 2009). His parameterization was published firstly in Berger (1978b), and after some years, a newer version in Berger and Loutre (1991) expanded the valid time range for ± 3 Myr. Now, in this chapter and the following, Berger (1978b) and Berger and Loutre (1991) will be referred to as Be78 and Be90, respectively.
 255 Both parameterizations, Be78 and Be90, are described in this section with the focus on the main formulas and tables presented in this classical paper.

Another remarkable researcher, Jacques Laskar, also simulated new long-term solutions for EOP. Berger used the Laskar solutions in Be90 (Laskar, 1986, 1988). Furthermore, within the last decades, Laskar published novel solutions focused on expanding the valid time range (e.g., Laskar et al., 1993, 2004, 2011). It's worth mentioning that although current computers
 260 can simulate the planetary motions around the Sun for billions of years, the chaotic behaviour of the solution still limits the validation to a few tens of millions of years (Laskar et al., 2011).

Table 1. The constant values are used to solve the Berger parameterizations.

	ε^* ($^\circ$)	$\bar{\psi}$ (arcsec)	ζ ($^\circ$)
Be78	23.320556	50.439273	3.392506
Be90	23.3334095	50.41726176	1.60075265

Thus, the efforts of André Berger and Jacques Laskar represent an important contribution to paleoclimatology. This way, following the idea of this chapter, the mathematical description of the Berger parameterizations, covering from equations to constants will be provided, as well as a Laskar custom parameterization, such as in the DINSOL source code.

265 1) The analytical solution of Be78 and Be90

Both parameterizations, Be78 and Be90, use spectral analysis, which used the same trigonometrical equations. However, Be78 and Be90 methods require distinctive data sources to work. Thus, DINSOL contains three tables for every Berger parameterization: obliquity, eccentricity, and precession, such as tables 1, 4, and 5 in Be78, respectively. Furthermore, all these data tables were obtained from an R package named PALINSOL (Crucifix, 2016), being converted to sequential binary files. The data con-
270 tained the following columns: amplitude, mean rate, phase, and period. The time in years for Be78 or Be90 parameterizations is represented in the equations by the t variable.

The calculation of the obliquity (ε) is then estimated with the equation:

$$\varepsilon = \varepsilon^* + \sum_{i=1}^N A_i \cos(R_i t + F_i) \quad (23)$$

where ε^* is a constant given in table 1, N representing the number of the terms per column, and A_i , R_i , and F_i are, respec-
275 tively: the second, third, and fourth columns of the obliquity tables used in Be78 and Be90. Similarly, to the obliquity, the eccentricity, e , can be calculated from the following equations:

$$e \sin \pi = \sum_{i=1}^N M_i \sin(G_i t + B_i) \quad (24)$$

$$e \cos \pi = \sum_{i=1}^N M_i \cos(G_i t + B_i) \quad (25)$$

280

$$e = \sqrt{(e \sin \pi)^2 + (e \cos \pi)^2} \quad (26)$$

where M_i , G_i , and B_i are, respectively: the second, third, and fourth columns of the eccentricity tables used in Be78 and Be90, and N is the number of elements per column. To calculate the precession, ϖ , the following these steps must be followed:

$$\psi = \bar{\psi} t + \zeta + \sum_{i=1}^N P_i \sin(K_i t + D_i) \quad (27)$$

285 being ψ the general precession, and $\bar{\psi}$ and ζ constants are given from table 1, as well as P_i , K_i , and D_i are, respectively: the second, third, and fourth columns of the precession tables used in Be78 and Be90. Moreover, N is the number of the table terms. Now, we also need to calculate the arctangent from $e \sin \pi$ and $e \cos \pi$, like the equation 28.

$$\arctan \pi = \arctan \left(\frac{e \sin \pi}{e \cos \pi} \right) \quad (28)$$

if $\arctan \pi$ is negative, 180° must be added for $\arctan \pi$ or else it must be kept unchanged. The longitude of the perihelion, ϖ ,
290 can now be calculated using the equation:

$$\varpi = \arctan \pi + \psi + \pi \quad (29)$$

If ϖ is greater than 360° , a subtraction: $\varpi - 360^\circ$, must be performed to obtain an angle less than the length of a full revolution. The longitude of perigee, ω , can be calculated as $\omega = \varpi + 180^\circ$. Additionally, it is crucial use the same units: radians, degrees, and arcseconds. For instance, DINSOL Berger subroutines convert all column data to radians.

295 2) The Laskar solutions

The DINSOL model combines two Laskar time series solutions, Laskar et al. (2004, 2011), resulting in a time range from -249 Myr to 21 Myr, referred to as the Lask. It implements the function $s(y)$, where y is a year multiple of thousand. However, if y is not a multiple of thousand, $s(y)$ cannot be used directly and a simple slope-intercept equation must be used where the two nearest points are defined as: before (t_i) and after (t_{i+1}). For instance, when $y = -4600$, then $t_i = -5000$ and $t_{i+1} = -4000$.
300 Thus, the effective time, t , used in the slope-intercept equation is $t = y - t_i$, which results in a time of $t = 400$.

Next, it is shown the Equation 30, where $f(y)$ may assume two forms:

$$f(y) = \begin{cases} s(y), & y \bmod 10^3 = 0 \\ \theta t + b, & y \bmod 10^3 \neq 0 \end{cases} \quad (30)$$

been $b = s(t_i)$ and slope given by:

$$\theta = \frac{s(t_{i+1}) - s(t_i)}{10^3} \quad (31)$$

305 The annual change for each EOP is small, resulting in a small calculation error from the slope-interception equation. Additionally, when the Be78 and Lask data calculated from DINSOL were compared, Figure 7 showed that the graphs overlap; therefore, the Lask parameterization can accurately estimate the nonexistent Laskar original data. Both Laskar solutions were obtained from the web page (<http://vo.imcce.fr/insola/earth/online/earth/earth.html>, last access: 21 January 2023) that is maintained by the Institut de Mécanique Céleste et de Calcul des Ephémérides (IMCCE).

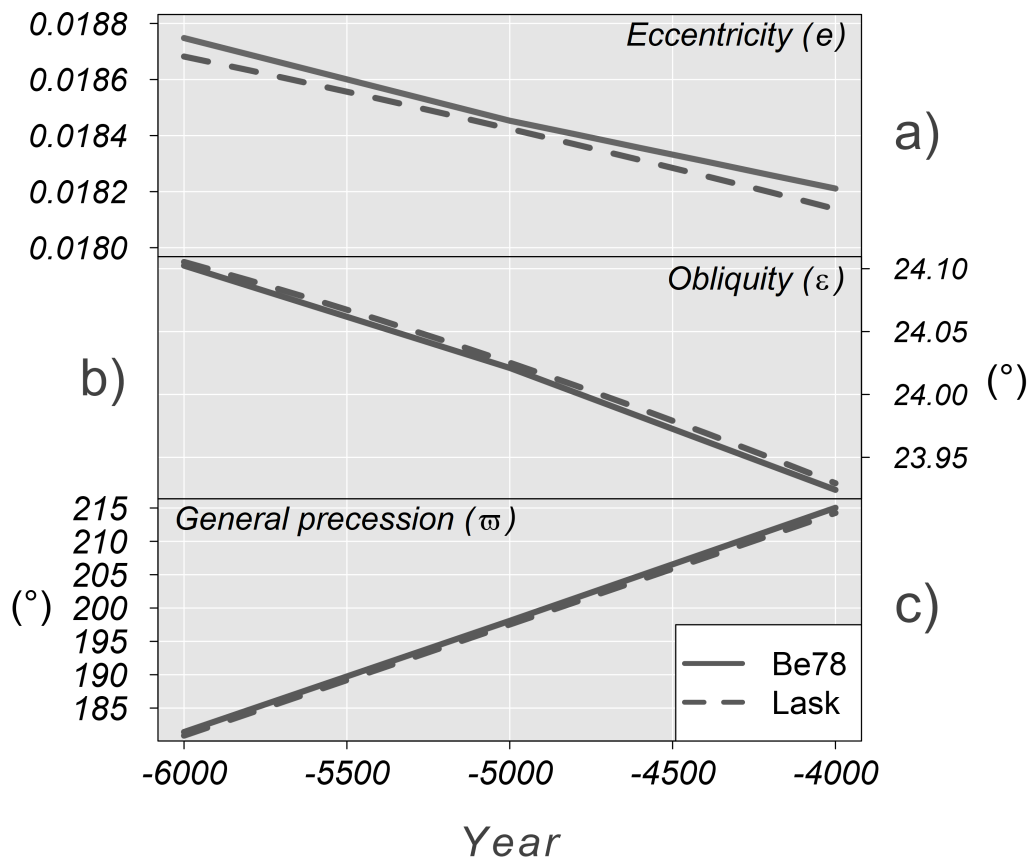


Figure 7. Comparison between Be78 and Lask data, with time (in years) on the horizontal axis. Additionally, graph (a) is eccentricity, (b) is obliquity [°], and (c) is precession [°].

310 2.5 Model structure, setup, and execution

The DINSOL source code has a simple hierarchical structure written in Fortran. A flow diagram representing the DINSOL source code is available in Figure 8, including input data, the main program, modules, functions, subroutines, and output data. The model initiates from the main program reading the input data: tables for analytical solutions of Be78 and Be90 and combined time series of Lask. The program also read data from the namelist file (Table 2) as well as a module containing the
315 declared variables and simulation parameters. In the next step, the program invokes the DINSOL subroutine, which is the main function and calls on all other functions for the simulations.

The next steps are a series of commands executed from the namelist setup function, where the calendar type must be initialised. Variables like spatial resolution, time interval, and calendar variables are then declared. The next step invokes parameterization to obtain the orbital parameters, and then the subroutines (seasons, perigee, and apogee) implement a calendar
320 function to determine the day and month occurrences of summer, autumn, winter, perihelion, and aphelion. The solar longitude subroutine is then called and computes the annual true solar longitude for use in the daily insolation and instantaneous irradiance subroutines. Finally, the output subroutine is responsible for storing the data simulated during the DINSOL execution.

The DINSOL model also works from a Graphical User Interface (GUI), where the namelist options are the same, except for the spatial resolution, where the GUI mode offers only six options: 5°, 4°, 3°, 2°, 1°, and 0.5°. All the output files generated
325 (Table 3) are identical regardless of the execution mode, except for the plot file *gui-plot.png*: a panel used to display results in the GUI mode. This plot contains sketches of the orbital parameters and contour fields for a simulated year: daily insolation, the difference to modern days, and the length of a day. A snapshot of the GUI interface and two graphical windows containing the results are displayed in Figure 9.

Users have the option to customise their simulation setup, implementing custom scenarios using *user-defined value*. The
330 orbital parameters can then be set without compliance to the Berger or Laskar parameterizations, provided that the results will not be invalidated. For instance, if the eccentricity is set to zero, the orbit of Earth would become a perfect circle, meaning the dates of perihelion and aphelion would no longer exist. If obliquity is set to zero, the seasons would not exist, and if a negative obliquity is assumed, the solstice and equinox dates would occur on inverted dates. Even under hypothetical cases, the program still works correctly.

Table 2. A short description of DINSOL namelist variables.

Variables	Short description
YEAR	Any integer number in the time-slice: -249 Myr to 21 Myr. <i>Note: zero is representing nowadays.</i>
S0	The solar constant in the range]0 : 10 ⁸ [. <i>Note: S0 must be in W/m²</i>
NY	Latitudinal number points.
NX	Longitudinal number points.
NTIME	The time interval within one day, given in hours or minutes: 1 - 6 hours 2 - 3 hours 3 - 1 hour 4 - 30 minutes 5 - 15 minutes
CALENDAR	Define the number of days in the year: 1 - 365 days 2 - 360 days
ORBITAL	Define the orbital parameterization: 1 - Be78: ± 1 Myr. 2 - Be90: ± 3 Myr. 3 - Lask: -249 Myr to 21 Myr. 4 - User-defined value.
ECC	Eccentricity: any value in the range [0:0.5].
OBLQ	Obliquity: any value in the range [-90:90].
PRCS	Precession: any value in the range [0:360[. <i>Note: This is the longitude of the perihelion, ϖ.</i>

Table 3. A short description of DINSOL output data.

Files	Short description
summary.txt	This file is a resume of the main results: <ul style="list-style-type: none">- Namelist setup- The orbital parameters- Astronomical dates- Annual average of daily insolation
insolation.txt	A formatted data containing some results in columns: <ul style="list-style-type: none">- Year- Days- True solar longitude (λ)- Relative Earth-sun distance (ρ)- Latitude (ϕ)- Solar declination (δ)- Day length (N)- Daily insolation (Q_0)
solar.radiation	A binary file of annual daily insolation (Q_0).
solar.radiation.ctl	A GrADS descriptor file.
radiation	A binary file of instantaneous solar radiation (Q_I).
radiation.ctl	A GrADS descriptor file.

Source code structure diagram
Daily Insolation (DINSOL-v1.0)
 Laboratory of Meteorology - LabMet
 Federal University of Vale do São Francisco - UNIVASF

These steps take crucial decisions from namelist values, affecting the output data directly. It is worth mentioning that we suppressed the **spatial resolution** because there are countless possibilities to set up the number of points of latitude and longitude. However, the graphical mode brings six options of spatial resolution: 5°, 4°, 3°, 2°, 1°, and 0.5° degrees. Furthermore, we have the **time interval** in hours and minutes, the **annual calendar**, and the methods to get the Earth's orbital parameters (each with 5, 2, and 4 options, respectively). Hence, the DINSOL offers many ways to run each simulation, and if we consider only the graphical mode, we have 240 different combinations.

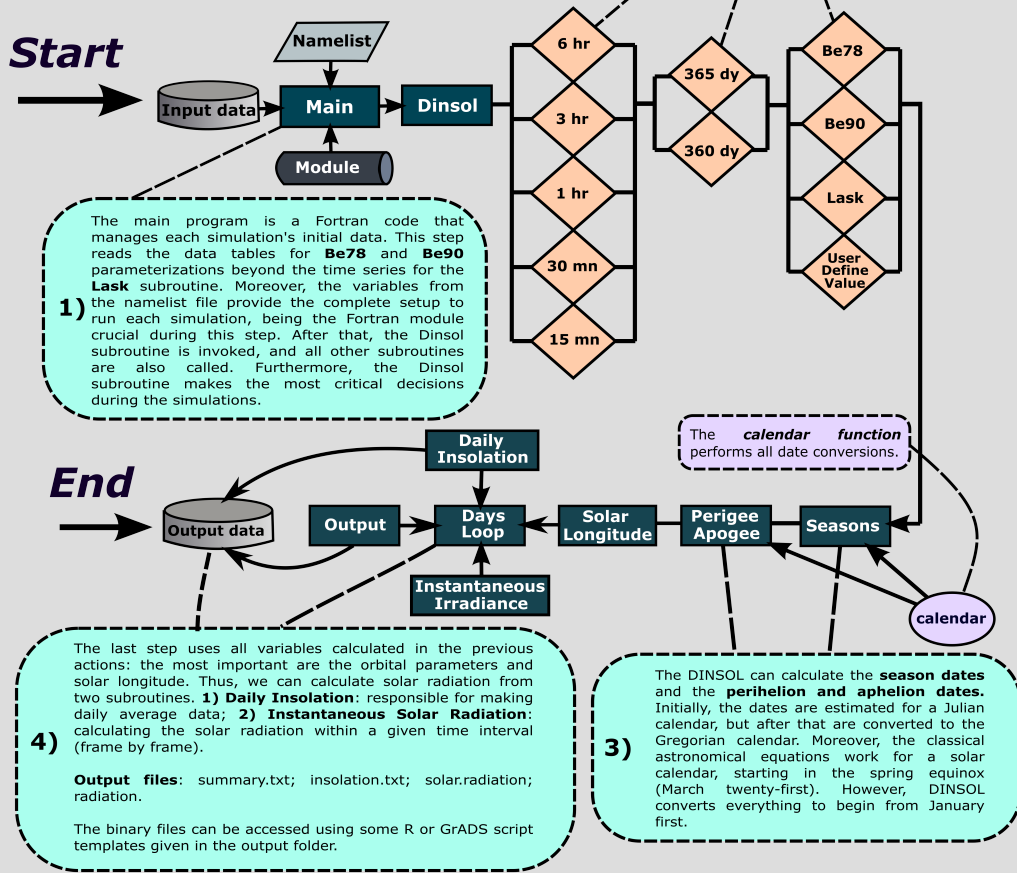


Figure 8. Fortran representation of the DINSOL source code, with subroutines, modules, namelist, input and output data and brief explanations of the simulation steps.

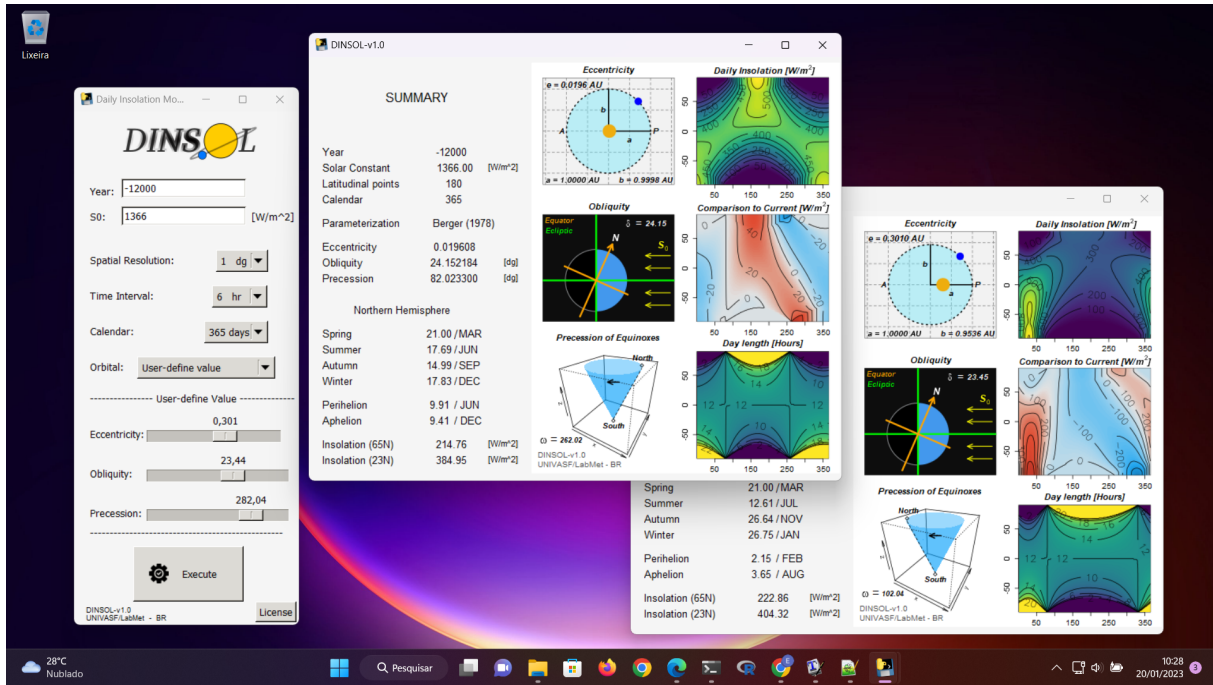


Figure 9. Snapshot of DINSOL-v1.0 GUI running on Windows 11.

345 3 Model evaluation: a short statistical analyse

This chapter evaluates the DINSOL program by comparing its products against data obtained from other similar tools or available in the literature. Still, the first subchapter brings the Earth's orbital parameters (EOP) evaluation, where Be78, Be90, and Lask parameterizations (chapter 2.4) were evaluated. For that, we compared the Be78 parameterization with the Goddard Institute for Space Studies (GISS) data computed by Bartlein and Shafer (2019). The GISS is a Fortran program that runs the EOP using Be78 parameterization. On the other hand, the Be90 and Lask parameterizations were evaluated by adopting the PALINSOL package (Crucifix, 2016). The EOP evaluation assumes a time series' starting from -150 kyr until the modern days, $t = 0$. Furthermore, we decided to use the climatic precession ($e \sin \varpi$) instead of the distance of perihelion, ϖ .

Over the following subchapters, we analysed the DINSOL compared to the PMIP2 and PALINSOL. At first, we evaluated the astronomical dates by using the PMIP2 dates as a reference. Please note that the classical method of measuring the paleo-climate dates assumes the spring equinox as a fixed date (March 21) and a constant month length regardless of the year. Still, in the final subchapter, the evaluation of the monthly insolation data was conducted where the assumption was that the solar constant was $S_0 = 1365 \text{ W m}^{-2}$; the year equal to zero $t = 0$ for modern days (0K); $t = -6000$ during the mid-Holocene (6K); and $t = -21000$ to last glacial maximum (21K); using a 365-day and 360-day calendar with the Berger (1978b) parameterizations (EOP and daily insolation) such as PMIP2 experiments implemented.

350 The samples were analysed from measures of central tendency using average (\bar{X}) and median (μ), also measures of dispersion using standard deviation (σ) and coefficient of variation (C_V). Additionally, the Root Mean Square Error (RMSE) was implemented to evaluate the sample differences, where the RMSE was calculated by performing the sum of the differences between simulation and observational data, given by equation 32:

$$RMSE = \sqrt{\frac{1}{N} \sum_{i=1}^N (S_i - O_i)^2} \quad (32)$$

365 conform Oliveira et al. (2019) N is the number of elements, S_i representing the simulation data, and O_i is the observational data. Noting that PMIP2, PALINSOL, and GISS are assumed as observational data, a standard dataset to evaluate the DINSOL.

3.1 Earth's orbital parameters

In Figure 10, there is a correlation between the GISS and DINSOL curves, indicating that DINSOL EOP subroutines (Be78, Be90, and Lask) function as expected. The error margin estimations were determined using a statistical summary shown in
 360 Table 4. Thus, measurements such as mean, \bar{X} , median, μ , standard deviation, σ , and coefficient of variation, C_V , indicate a strong correlation between DINSOL and GISS as well as the DINSOL and PALINSOL. Therefore, suggesting an insignificant difference to the EOP DINSOL products. The RMSE values also support the previous statistical inference from the insignificant difference between the samples.

The GISS and Be78 values are nearly identical, which validates the Be78 subroutine. The same occurs with Be90 and
 365 Lask parameterizations, where the test parameters indicate a roundoff error between the DINSOL and PALINSOL. In addition, about the coefficient of variation, C_V , we can realize that the climatic precession ($e \sin \varpi$) was who showed the more prominent differences. Moreover, we found the major RMSE value during the Lask evaluation, specifically in the obliquity (ε) parameter. Note that for negative years (reconstructions), the DINSOL assumes Laskar et al. (2011) (1a10), while the PALINSOL adopts Laskar et al. (2004) (1a04), which justifies this slight difference.

370 Although the parameterizations Be78, Be90, and Lask provide almost the same values, the users need to pay attention to the epoch and ecliptic reference used by each parameterization, that is, the time reference, which is different from one another. For instance, while Be78 assumed 1950 as the epoch and 1850 as its ecliptic reference, Lask parameterization adopted J2000 as a time reference, conforming to the Julian calendar. Therefore, $t = 0$ represents the year 1950 in Be78 and 2000 in Lask. Thus, to overlap the Be78 and Lask parameterizations, we would need to perform a calibration shift of 50 years one another.
 375 For additional information is recommended to read the Berger and Laskar articles.

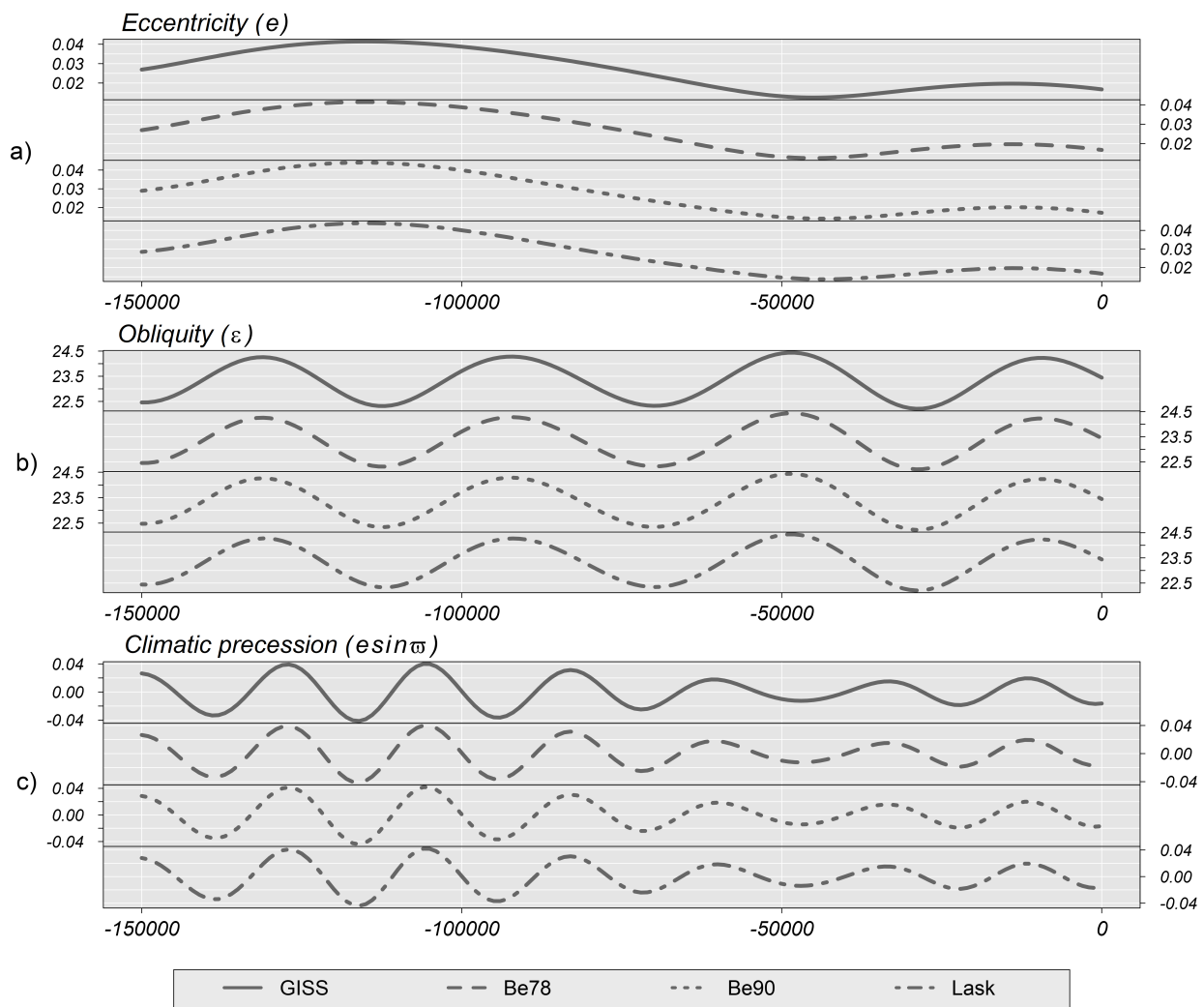


Figure 10. Time series of the Earth's orbital parameters (EOP) for the last 150 kyr. a) Eccentricity, b) Obliquity and c) Climatic precession. Each graph brings Goddard Institute for Space Studies (GISS) and DINSOL parameterizations: Be78, Be90, and Lask.

Table 4. Evaluation of the DINSOL model adopting a statistical analysis from Earth’s Orbital Parameters (EOP), where the values were from minima each tool type (*Min*), the maxima (*Max*), average (\bar{X}), median (μ), standard deviation (σ), coefficient of variation (C_V), and the root mean square error (*RMSE*). All presented data were obtained from DINSOL, GISS, and PALINSOL. Where the EOP are the eccentricity (e), obliquity (ε), and climatic precession ($e \sin \varpi$).

		<i>Min</i>	<i>Max</i>	\bar{X}	μ	σ	C_V	<i>RMSE</i>
Be78	GISS [e]	0.012509	0.041421	0.026755	0.026859	0.010076	0.37660	7.3008E-09
	DINSOL [e]	0.012509	0.041421	0.026755	0.026859	0.010076	0.37660	
	GISS [ε]	22.20748	24.43585	23.35631	23.44278	0.711554	0.03047	1.3622E-06
	DINSOL [ε]	22.20748	24.43585	23.35631	23.44278	0.711554	0.03047	
	GISS [$e \sin \varpi$]	-0.0413	0.039898	-0.000147	-0.000187	0.020279	-137.686	3.094E-08
	DINSOL [$e \sin \varpi$]	-0.0413	0.039898	-0.000147	-0.000187	0.020279	-137.682	
Be90	PALINSOL [e]	0.014093	0.043988	0.027717	0.026111	0.01043	0.376280	6.5272E-09
	DINSOL [e]	0.014093	0.043988	0.027717	0.026111	0.01043	0.376280	
	PALINSOL [ε]	22.23484	24.43667	23.36954	23.43276	0.702570	0.03007	1.4389E-06
	DINSOL [ε]	22.23484	24.43667	23.36954	23.43276	0.702570	0.03007	
	PALINSOL [$e \sin \varpi$]	-0.043938	0.041798	-0.000131	-5.717E-05	0.021009	-160.7944	4.0904E-08
	DINSOL [$e \sin \varpi$]	-0.043938	0.041798	-0.000131	-5.717E-05	0.021009	-160.7965	
Lask	PALINSOL [e]	0.013706	0.043921	0.027408	0.025952	0.010528	0.384112	3.0026E-07
	DINSOL [e]	0.013706	0.043921	0.027408	0.025952	0.010528	0.384112	
	PALINSOL [ε]	22.20721	24.43463	23.35852	23.43069	0.70934	0.030368	1.5292E-05
	DINSOL [ε]	22.20721	24.43464	23.35852	23.43071	0.70934	0.030368	
	PALINSOL [$e \sin \varpi$]	-0.043845	0.041907	-0.000132	-0.000386	0.020825	-158.3981	2.2275E-07
	DINSOL [$e \sin \varpi$]	-0.043845	0.041907	-0.000132	-0.000386	0.020825	-158.3987	

Table 5. This table contains the dates of summer, autumn, winter, perihelion, and aphelion during the modern days (0K), mid-Holocene (6K), and last glacial maximum (21K) calculated by DINSOL and by PMIP2, both using the method of Be78, for 365-day and 360-day calendars.

		Summer solstice (June)	Autumnal equinox (September)	Winter solstice (December)	Perihelion	Aphelion
0K	PMIP2 [365]	21.73	23.30	22.05	2.85/01	4.35/07
	DINSOL [365]	21.74	23.30	22.05	2.85/01	4.35/07
	PMIP2 [360]	22.46	24.74	23.26	4.91/01	4.91/07
	DINSOL [360]	22.47	24.76	23.28	4.91/01	4.91/07
6K	PMIP2 [365]	22.45	19.56	17.61	20.42/09	21.92/03
	DINSOL [365]	22.46	19.57	17.62	20.42/09	21.92/03
	PMIP2 [360]	23.17	21.06	18.89	21.90/09	21.90/03
	DINSOL [360]	23.18	21.07	18.91	21.90/09	21.90/03
21K	PMIP2 [365]	21.32	23.52	22.65	15.51/01	17.01/07
	DINSOL [365]	21.32	23.52	22.65	15.51/01	17.01/07
	PMIP2 [360]	22.06	24.96	23.86	17.39/01	17.39/07
	DINSOL [360]	22.06	24.97	23.87	17.39/01	17.39/07

3.2 Astronomical dates

Table 5 contains the dates of summer, autumn, winter, perihelion, and aphelion calculated by DINSOL and PMIP2, where both use the method of Be78. These dates represent the modern days (0K), mid-Holocene (6K), and last glacial maximum (21K). Thus, perihelion and aphelion dates calculated by DINSOL are identical to those calculated by PMIP2. These dates correlate with the expected dates because they were determined using equations 4, 5, and 6. Nevertheless, the summer, autumn, and winter dates have a small error to the PMIP2-determined. In the DINSOL, these dates were estimated from a large number of values within the annual true solar longitude vector. In table 5, an accumulative error is observed, where the season date error increases as a function of the distance to the spring equinox. The RMSE provides values around 12, 16, and 19 min for summer, autumn, and winter, respectively. Thus, for lesser than 20 min, the error remains small, meaning that the DINSOL provides accurate date estimates. The compliance of DINSOL and PMIP2 to the classical method of measuring astronomical events must always be considered. However, for a more realistic approach to paleoclimate calendars, it is recommended to follow the methodology of Joussaume and Braconnot (1997) or Bartlein and Shafer (2019), although many authors prefer the classical method because it is easier to compare with our current Gregorian calendar.

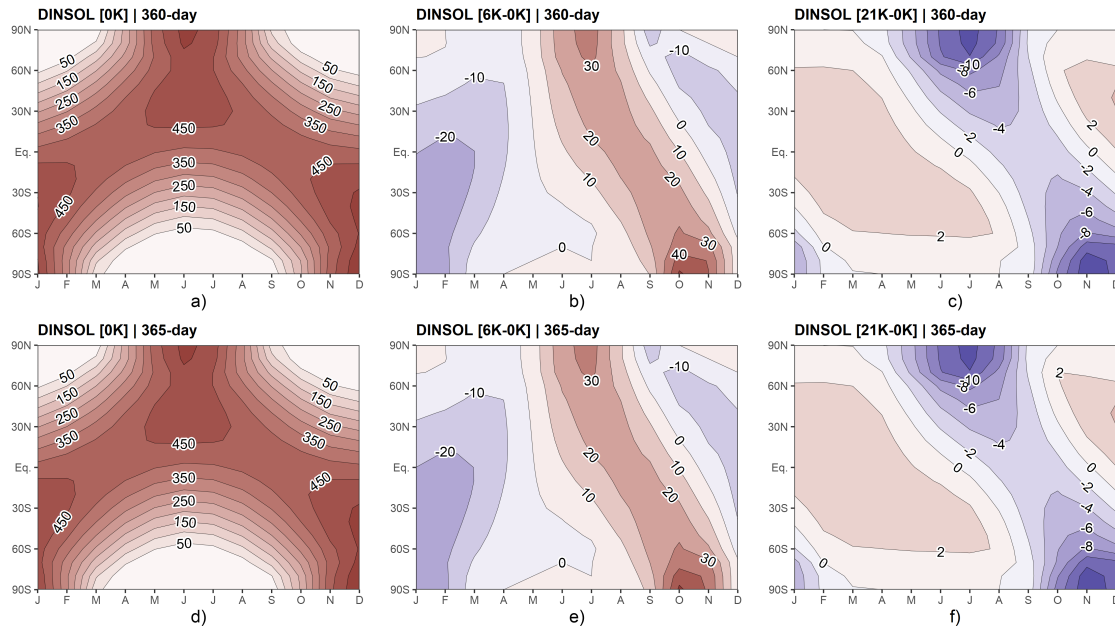


Figure 11. DINSOL monthly insolation contour fields obtained from a 360-day calendar: a) Modern days, b) mid-Holocene minus modern days, c) Last maximum glacial minus modern days, and from a 365-days: d) Modern days, e) mid-Holocene minus modern days, f) Last maximum glacial minus modern days. The horizontal axis represents the months, while the vertical axis is the latitude.

3.3 Monthly insolation

390 The DINSOL monthly insolation was analysed from a visual evaluation of the contour fields (Figures 11, 12, 13) and some statistical parameters (Table 6). This evaluation used PMIP2 insolation samples prepared from 365-day and 360-day calendars at three different periods: modern days (0K), mid-Holocene (6K-0K), and last glacial maximum (21K-0K). Simulations were thus performed with DINSOL using the same PMIP2 setup. Additionally, the DINSOL was compared to the monthly insolation obtained from the PALINSOL package, but, in this case, we considered only the last glacial maximum (21K-0K) period.

395 Incidentally, the contour fields present in Figure 11 (a-c) were generated using a 360-day calendar, with (d - f) employing a 365-day calendar setup. From Figure 11, compared to the modern days, the biggest insolation differences were found during the mid-Holocene, primarily due to the perihelion date changes, around January 3 to modern days and September 20 during the mid-Holocene. This analysis of the mid-Holocene agrees with the presented discussion in Brierley et al. (2020).

In order to perform the visual evaluation, we plotted the contour fields of the DINSOL minus PMIP2 (Figure 12). Thus, 400 in Figure 12 (a-c), we have contour fields made from a 360-day calendar, whereas Figure 12 (d-f) was built from a 365-day calendar. Still, it is clear that to the modern days (0K), mid-Holocene (6K), and last glacial maximum (21K), the differences are within the roundoff error, about $\pm 0.08 \text{ W m}^{-2}$. Figure 12 (a, b, and e) contains plots almost uniform with values nearest to zero than the other pictures. For example, Figure 12-d presents a more remarkable bias. However, it is worth noticing that the

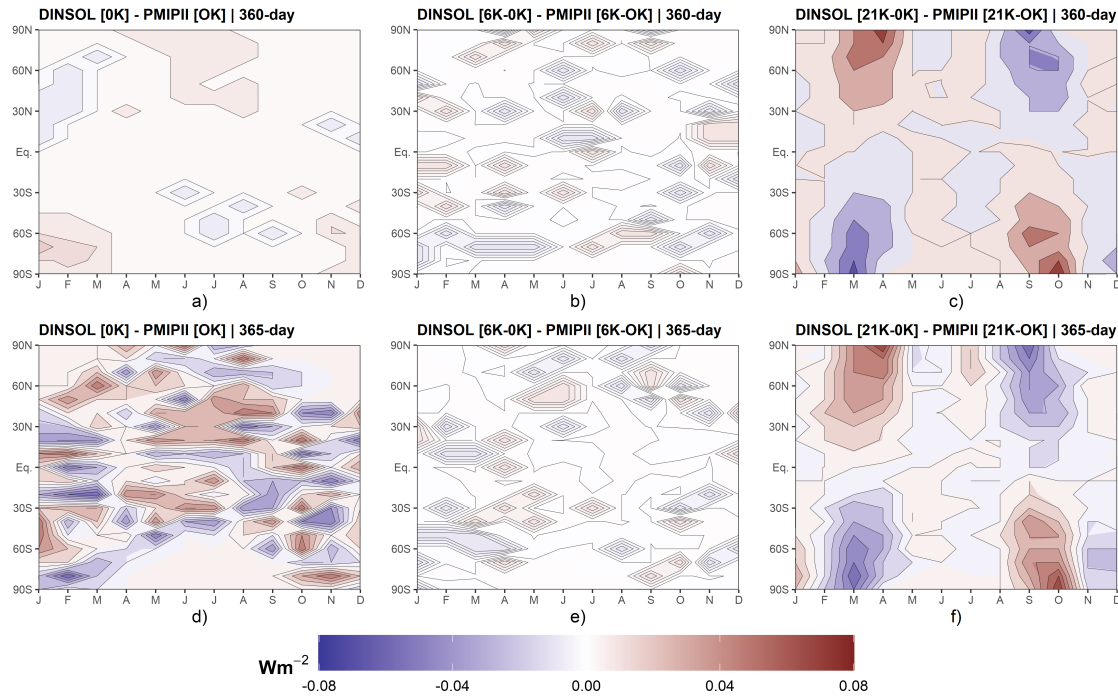


Figure 12. Monthly insolation differences between DINSOL and PMIP2 from a 360-day calendar: a) Modern days, b) mid-Holocene minus modern days, c) Last maximum glacial minus modern days, and from a 365-days calendar: d) Modern days, e) mid-Holocene minus modern days, f) Last maximum glacial minus modern days. The horizontal axis represents the months, while the vertical axis is the latitude.

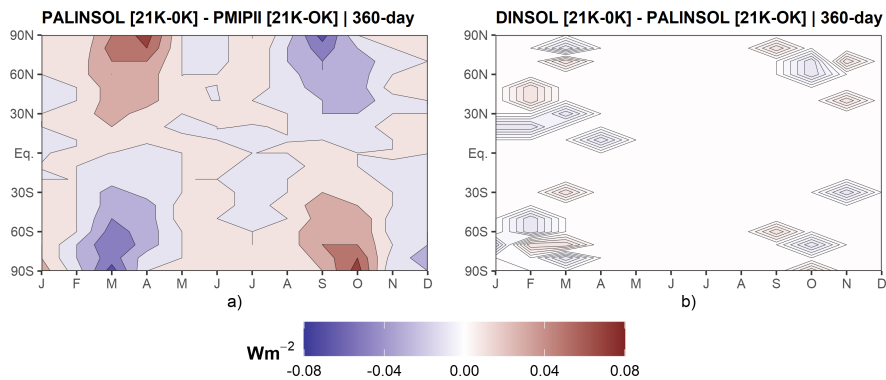


Figure 13. Monthly insolation from Last maximum glacial minus modern days contour fields: a) PALINSOL minus PMIP2, and b) DINSOL minus PALINSOL. Each one is for a 360-day calendar. The horizontal axis represents the months, while the vertical axis is the latitude.

values are randomly distributed in the image, which is considered normal and allows us to infer that the DINSOL is working as the expectations in the modern days (0K) and mid-Holocene (6K), including both calendar options: 360 and 365-days.

405

On the other hand, Figure 12 (c and f) shows a systematic bias for high latitudes, where we can observe an almost harmonic behaviour between the northern and southern hemispheres, precisely closer to the equinoxes dates. Despite that, the differences remain small, and as a confirmation test, we decided, additionally, to compare the PMIP2 (21K-0K) against the PALINSOL. Moreover, we also performed a DINSOL and PALINSOL comparison to the last glacial maximum. Thus, Figure 410 13-a showed the same pattern at high latitudes, whereas Figure 13-b plotted an almost uniform field. Therefore, the DINSOL minus PALINSOL works as expected, suggesting that the PMIP2 (21K-0K) contains some systematic roundoff error in their monthly insolation files, which should be reported to the PMIP team in order to investigate it.

With regard to the statistical analyses, the parameters available in table 6 are dependable enough to confirm or reject our previous visual analyses from Figures (11, 12, and 13). At first, we can see that the minima and maxima are nearly identical and 415 converge towards the same value in the mid-Holocene. Furthermore, the central tendency indicates that all samples' average values are equal, while most median values are almost identical. The dispersion values also corroborate the previous conclusions, where the standard deviation and coefficient of variation suggest no significant differences. Still, in order to estimate the error between DINSOL and PMIP2 samples, we also compute the RMSE. Table 6 shows that the major value occurred from a calendar of 365 days when assayed the modern days, 0.02595 Wm^{-2} . On the other hand, the lesser RMSE value was found 420 for a calendar of 360 days by considering the mid-Holocene sample.

As a final analysis, we will focus on the last glacial maximum, including the PALINSOL package as an alternative to the PMIP2 samples. Thus, comparing PALINSOL and PMIP2, we realized that the RMSE was almost identical to the DINSOL and PMIP2 values. However, evaluating the DINSOL from the PALINSOL, we got an RMSE of 0.00324 Wm^{-2} , which is around 84% less than the value obtained from DINSOL and PMIP2 analyses. Therefore, it is reasonable to claim that the 425 DINSOL program can compute the daily insolation accurately compared to the literature because the field differences show us an almost homogenous contour data with values near zero. Indeed, according to Table 6, all samples must be considered numerically the same because we did not find significant differences in our statistical analyses.

Table 6. Evaluation of the DINSOL model adopting a statistical analysis from monthly insolation data samples, where the data displayed represents the minimum values of each data (*Min*), the maximum values (*Max*), average (\bar{X}), median (μ), standard deviation (σ), coefficient of variation (C_V), and the root mean square error (*RMSE*). All presented data were obtained from DINSOL, PMIPII, and PALINSOL. They have two calendar options (365 and 360 days) and three different periods: modern days (0K), mid-Holocene (6K-0K), and last glacial maximum (21K-0K).

		<i>Min</i>	<i>Max</i>	\bar{X}	μ	σ	C_V	<i>RMSE</i>
0K	DINSOL [365]	0	550.39	292.58	341.62	169.3383	0.5788	0.02595
	PMIPII [365]	0	550.40	292.58	341.60	169.3369	0.5788	
	DINSOL [360]	0	548.26	292.62	341.41	169.4682	0.5791	0.00481
	PMIPII [360]	0	548.25	292.62	341.41	169.4666	0.5791	
6K-0K	DINSOL [365]	-25.50	52.14	1.0466	-0.081	16.0434	15.3283	0.00313
	PMIPII [365]	-25.50	52.14	1.0466	-0.085	16.0435	15.3288	
	DINSOL [360]	-25.61	51.83	1.15	-0.15	16.0347	13.9873	0.00290
	PMIPII [360]	-25.61	51.83	1.15	-0.16	16.0347	13.9854	
21K-0K	DINSOL [365]	-13.56	4.16	-0.83	0	4.0808	-4.9441	0.01966
	PMIPII [365]	-13.54	4.15	-0.83	0	4.0812	-4.9456	
	DINSOL [360]	-13.48	4.15	-0.84	0	4.0870	-4.8427	0.02054
	PMIPII [360]	-13.46	4.15	-0.84	0	4.0876	-4.8424	
	PALINSOL [360]	-13.48	4.15	-0.84	0	4.0870	-4.8433	0.02043
	DINSOL [360]	-	-	-	-	-	-	0.00324

4 Conclusions

The Daily Insolation (DINSOL-v1.0) program is a robust and versatile tool offering various simulation options and usabilities. It is ideal to compute solar radiation data for climate models, which aids in simplified climate approaches or more complex studies. Furthermore, the DINSOL model may be employed as an educational tool adopting its friendly graphical user interface (GUI). The program was developed as a novel educational tool for use in geosciences colleges worldwide, providing a quick view of daily insolation by considering the Milankovitch cycles (ideal for paleoclimatology) or adopting hypothetical orbital parameters (ideal for exoplanets). Therefore, the program can aid students, teachers, and researchers in conducting their respective studies. Still, despite the program evaluation having presented insignificant differences compared to the literature, the users are incentivised to report any find issues during the program execution. Moreover, DINSOL is an open-source program whose author encourages users to develop the source code continuously. Ultimately, the DINSOL may be considered a viable tool that accurately provides various types of output data, such as the Earth's orbital parameters, astronomical dates, daily insolation, and instantaneous solar radiation, simulating the passage of day to night realistically.

Code and data availability. The DINSOL program is available for download in different repositories: Zenodo, GitHub, and LabMet/UNIVASF. Further, even though the program is a Linux/Unix software, a custom Windows OS version is available too. Both versions (Windows and Linux) contain manuals and README files to aid users in installing the dependencies and compiling the source code. On Zenodo, the Windows version is available in (<https://doi.org/10.5281/zenodo.7554620>, last access: 20 January 2023), while the Linux version in (<https://doi.org/10.5281/zenodo.7551458>, last access: 20 January 2023). Still, GitHub provides only the Linux version: (<https://github.com/Emerson-D-Oliveira/dinsol-v1.0-linux>, last access: 20 January 2023). In addition, both programs are available on LabMet/UNIVASF webpage in (<http://labmet.univasf.edu.br/joomla/index.php/pesquisas/modelos-numericos>, last access: 20 January 2023). It is important to mention that the Windows version does not require any prior programming experience from the user to install and execute the DINSOL from the GUI mode. Moreover, although the program has not been tested on macOS, the Linux version should work since some adjustments to be adopted. Ultimately, users are encouraged to adapt and share the modified source code with the community.

Sample availability. A supplementary file containing all datasets used to prepare this manuscript is available in the Zenodo repository (<https://doi.org/10.5281/zenodo.7557354>, last access: 21 January 2023).

Appendix A: Data manipulation

The output folder contains five scripts to aid users in analysing the simulation data. The files are listed with a brief description in Table A1.

Table A1. Brief description of all scripts located in the DINSOL output folder.

Scripts	Short description
get-dinsol-value.R	This script provides the insolation and day length from a given day and latitude. Moreover, this script still plots a panel containing six graphs.
plot-dinsol.R	This script makes a plot with contour fields of the daily insolation.
plot-dinsol.gs	This script makes a plot with contour fields of the daily insolation.
plot-global.R	This script makes a plot of the instantaneous solar radiation globally from a given day and hour.
plot-radiation.gs	This last script makes an animation using the GrADS graphical window.

455 **Appendix B: Computing power**

The DINSOL does not adopt restrictions for latitudinal and longitudinal number points during execution by command lines, which means that the high-resolution setups demand users' attention. This appendix brings a table containing the output file sizes for different simulation setups, where the instantaneous solar radiation file (*radiation*) grows significantly as a function of the time interval (hours or minutes) and spatial resolution. Thus, it is necessary to ensure that the computer has sufficient storage capacity in its hard disk when prior to conducting a high-resolution simulation; otherwise, the system could crash, interrupting the simulation. It is worth mentioning that most data visualization tools cannot allocate enormous files. Thus, to get around it, the user should use some tool like the Climate Data Operator (CDO) to extract a specific day-hour and perform some plot analysis posteriorly. Another question is the execution time, which is increasing substantially and is a function of the computational power, compiler, program setup, etc. In addition, even though the standard source code works only in serial execution, the author already adapted and tested the code to work in parallel using the OpenMP API, which improved the program performance significantly. Please note that when the *radiation* file is not required, the simulation parameters can be set to NX=1 and NTIME=1, allowing users to change the values of NY while keeping simulation times minimal. In any case,

Table B1. DINSOL short performance summary by considering the spatial resolution and time interval changes, where the computation was performed in the Ubuntu OS using the IFORT 13 compiler. Thus, we have the required machine storage for each output file as well as the execution time.

		<i>6 hours</i>	<i>1 hour</i>	<i>15 minutes</i>
<hr/>				
	<i>insolation.txt[MB]</i>	5.7	5.7	5.7
<hr/>				
1.0°	<i>solar.radiation[MB]</i>	1.10	1.10	1.10
<hr/>				
	<i>radiation[GB]</i>	1.5	8.5	34.0
<hr/>				
	Execution time[min]	0.30	1.17	5.05
<hr/>				
	<i>insolation.txt[MB]</i>	12.0	12.0	12.0
<hr/>				
0.5°	<i>solar.radiation[MB]</i>	2.10	2.1	2.1
<hr/>				
	<i>radiation[GB]</i>	5.70	34.0	136.0
<hr/>				
	Execution time[min]	0.78	5.10	19.47
<hr/>				

the most efficient option would be to modify the source code, deactivating the instantaneous solar radiation subroutine and not storing the *radiation* data.

470 *Author contributions.* Oliveira E.D wrote independently all DINSOL source code, scripts, manuals, as well as this manuscript.

Competing interests. The author declares that have no conflict of interest.

Acknowledgements. We thank Michel Crucifix, André Berger, and Jacques Laskar for providing the input data used in DINSOL parameterizations. In addition, we also thank Patrick Bartlein for providing the time series of the Earth's orbital parameters, the Paleoclimate Modelling Intercomparison Project (PMIP) team for providing the monthly insolation data, and the PALINSOL author once the package was crucial to
475 perform a confirmation test. We also thank Kevin Schwarzwald and the referees for the valuable comments regarding the software and the article during the public discussion stage. Their suggestions and observations were fundamental to improving the article's quality. Moreover, we are grateful to the topical editor Travis O'Brien and the whole journal editorial team. Ultimately, we thank the Federal University of Vale do São Francisco (UNIVASF) and the Laboratory of Meteorology (LabMet) for incentivising the development of the DINSOL-v1.0.

References

- 480 Bartlein, P. J. and Shafer, S. L.: Paleo calendar-effect adjustments in time-slice and transient climate-model simulations (PaleoCalAdjust v1.0): impact and strategies for data analysis, *Geoscientific Model Development*, 12, 3889–3913, <https://doi.org/10.5194/gmd-12-3889-2019>, 2019.
- Berger, A.: Obliquity and general precession for the last 5 000 000 years, *Astron. Astrophys*, 51, 127–135, 1976.
- Berger, A.: Long-term variations of the Earth's orbital elements, *Celestial Mech*, 15, 53–74, 1977.
- 485 Berger, A.: Long-term variations of daily insolation and Quaternary, *J. Atmos. Sci*, 35, 2362–2367, 1978a.
- Berger, A.: Long-term variations of caloric insolation resulting from the Earth's orbital elements, *Quaternary Res*, 9, 139–167, 1978b.
- Berger, A.: Milankovitch, the father of paleoclimate modeling, *Climate of the Past*, 17, 1727–1733, <https://doi.org/10.5194/cp-17-1727-2021>, 2021.
- Berger, A. and Loutre, M.: Insolation values for the climate of the last 10 million years, *Quaternary Science Reviews*, 10, 297–317, [https://doi.org/https://doi.org/10.1016/0277-3791\(91\)90033-Q](https://doi.org/https://doi.org/10.1016/0277-3791(91)90033-Q), 1991.
- 490 Berger, A., Loutre, M.-F., and Yin, Q.: Total irradiation during any time interval of the year using elliptic integrals, *Quaternary Science Reviews*, 29, 1968–1982, <https://doi.org/https://doi.org/10.1016/j.quascirev.2010.05.007>, 2010.
- Beutler, G.: *Methods of Celestial Mechanics*, Springer Berlin, Heidelberg, <https://doi.org/10.1007/b138225>, 2005.
- Borkowski, K. M.: The Persian Calendar for 3000 Years, *Earth, Moon and Planets*, 74, 223–230, <https://doi.org/https://doi.org/10.1007/BF00055188>, 1996.
- 495 Brierley, C. M., Zhao, A., Harrison, S. P., Braconnot, P., Williams, C. J. R., Thornalley, D. J. R., Shi, X., Peterschmitt, J.-Y., Ohgaito, R., Kaufman, D. S., Kageyama, M., Hargreaves, J. C., Erb, M. P., Emile-Geay, J., D'Agostino, R., Chandan, D., Carré, M., Bartlein, P. J., Zheng, W., Zhang, Z., Zhang, Q., Yang, H., Volodin, E. M., Tomas, R. A., Routsou, C., Peltier, W. R., Otto-Bliesner, B., Morozova, P. A., McKay, N. P., Lohmann, G., Legrande, A. N., Guo, C., Cao, J., Brady, E., Annan, J. D., and Abe-Ouchi, A.: Large-scale features and evaluation of the PMIP4-CMIP6 *midHolocene* simulations, *Climate of the Past*, 16, 1847–1872, <https://doi.org/10.5194/cp-16-1847-2020>, 2020.
- 500 Crucifix, M.: palinsol : a R package to compute Incoming Solar Radiation (insolation) for palaeoclimate studies, Zenodo, <https://doi.org/10.5281/zenodo.7198545>, 2016.
- Crucifix, M., Claussen, M., Ganssen, G., Guiot, J., Guo, Z., Kiefer, T., Loutre, M.-F., Rousseau, D.-D., and Wolff, E.: Preface "Climate change: from the geological past to the uncertain future – a symposium honouring André Berger", *Climate of the Past*, 5, 707–711, <https://doi.org/10.5194/cp-5-707-2009>, 2009.
- 505 Eyring, V., Bony, S., Meehl, G. A., Senior, C. A., Stevens, B., Stouffer, R. J., and Taylor, K. E.: Overview of the Coupled Model Intercomparison Project Phase 6 (CMIP6) experimental design and organization, *Geoscientific Model Development*, 9, 1937–1958, <https://doi.org/10.5194/gmd-9-1937-2016>, 2016.
- 510 Fischer, H., van den Broek, K. L., Ramisch, K., and Okan, Y.: When IPCC graphs can foster or bias understanding: evidence among decision-makers from governmental and non-governmental institutions, *Environmental Research Letters*, 15, 114041, <https://doi.org/10.1088/1748-9326/abbc3c>, 2020.
- Fu, W. Q.: 4 - Radiative Transfer, in: *Atmospheric Science (Second Edition)*, edited by Wallace, J. M. and Hobbs, P. V., pp. 113–152, Academic Press, San Diego, second edition edn., <https://doi.org/https://doi.org/10.1016/B978-0-12-732951-2.50009-0>, 2006.
- 515 Hamilton, D. P.: Fresh solutions to the four-body problem, *Nature*, 533, 187–188, <https://doi.org/https://doi.org/10.1038/nature17896>, 2016.

- Hartmann, D. L.: Global Physical Climatology (Second Edition), Elsevier Science, <https://doi.org/10.1016/C2009-0-00030-0>, 2016.
- Joussaume, S. and Braconnot, P.: The Persian Calendar for 3000 Years, *Journal of Geophysical Research*, 102, 1943–1956, <https://doi.org/https://doi.org/10.1029/96JD01989>, 1997.
- Jungclaus, J. H., Bard, E., Baroni, M., Braconnot, P., Cao, J., Chini, L. P., Egorova, T., Evans, M., González-Rouco, J. F., Goosse, H.,
520 Hurtt, G. C., Joos, F., Kaplan, J. O., Khodri, M., Klein Goldewijk, K., Krivova, N., LeGrande, A. N., Lorenz, S. J., Luterbacher, J., Man,
W., Maycock, A. C., Meinshausen, M., Moberg, A., Muscheler, R., Nehrbass-Ahles, C., Otto-Bliesner, B. I., Phipps, S. J., Pongratz, J.,
Rozanov, E., Schmidt, G. A., Schmidt, H., Schmutz, W., Schurer, A., Shapiro, A. I., Sigl, M., Smerdon, J. E., Solanki, S. K., Timmreck,
C., Toohey, M., Usoskin, I. G., Wagner, S., Wu, C.-J., Yeo, K. L., Zanchettin, D., Zhang, Q., and Zorita, E.: The PMIP4 contribution to
CMIP6 – Part 3: The last millennium, scientific objective, and experimental design for
525 the PMIP4 *past1000* simulations, *Geoscientific Model Development*, 10, 4005–4033, <https://doi.org/10.5194/gmd-10-4005-2017>, 2017.
- Kageyama, M., Braconnot, P., Harrison, S. P., Haywood, A. M., Jungclaus, J. H., Otto-Bliesner, B. L., Peterschmitt, J.-Y., Abe-Ouchi, A.,
Albani, S., Bartlein, P. J., Brierley, C., Crucifix, M., Dolan, A., Fernandez-Donado, L., Fischer, H., Hopcroft, P. O., Ivanovic, R. F.,
Lambert, F., Lunt, D. J., Mahowald, N. M., Peltier, W. R., Phipps, S. J., Roche, D. M., Schmidt, G. A., Tarasov, L., Valdes, P. J., Zhang, Q.,
and Zhou, T.: The PMIP4 contribution to CMIP6 – Part 1: Overview and over-arching analysis plan, *Geoscientific Model Development*,
530 11, 1033–1057, <https://doi.org/10.5194/gmd-11-1033-2018>, 2018.
- Klippel, L., St. George, S., Büntgen, U., Krusic, P. J., and Esper, J.: Differing pre-industrial cooling trends between tree rings and lower-
resolution temperature proxies, *Climate of the Past*, 16, 729–742, <https://doi.org/10.5194/cp-16-729-2020>, 2020.
- Kostadinov, T. S. and Gilb, R.: Earth Orbit v2.1: a 3-D visualization and analysis model of Earth’s orbit, Milankovitch cycles and insolation,
Geoscientific Model Development, 7, 1051–1068, <https://doi.org/10.5194/gmd-7-1051-2014>, 2014.
- 535 Laskar, J.: Secular terms of classical planetary theories using the results of general theory, *Astronomy and Astrophysics*, 157, 59–70, 1986.
- Laskar, J.: Secular evolution of the solar system over 10 million years, *Astronomy and Astrophysics*, 198, 341–362, 1988.
- Laskar, J., Joutel, F., and Boudin, F.: Orbital, precessional, and insolation quantities for the earth from -20 Myr to +10 Myr., *Astronomy and
Astrophysics*, 270, 522–533, 1993.
- Laskar, J., Robutel, P., Joutel, F., Gastineau, M., Correia, A. C. M., and Levrard, B.: A long-term numerical solution for the insolation
540 quantities of the Earth, *Astronomy and Astrophysics*, 428, 261–285, <https://doi.org/https://doi.org/10.1051/0004-6361:20041335>, 2004.
- Laskar, J., Fienga, A., Gastineau, M., and Manche, H.: La2010: a new orbital solution for the long-term motion of the Earth, *Astronomy and
Astrophysics*, 532, 1–15, <https://doi.org/https://doi.org/10.1051/0004-6361/201116836>, 2011.
- Lhardy, F., Bouttes, N., Roche, D. M., Abe-Ouchi, A., Chase, Z., Crichton, K. A., Ilyina, T., Ivanovic, R., Jochum, M., Kageyama, M.,
Kobayashi, H., Liu, B., Menviel, L., Muglia, J., Nuterman, R., Oka, A., Vettoretti, G., and Yamamoto, A.: A First Intercomparison of the
545 Simulated LGM Carbon Results Within PMIP-Carbon: Role of the Ocean Boundary Conditions, *Paleoceanography and Paleoclimatology*,
36, <https://doi.org/https://doi.org/10.1029/2021PA004302>, 2021.
- Liou, K. N.: An Introduction to Atmospheric Radiation, Academic Press, [https://www.sciencedirect.com/bookseries/
international-geophysics/vol/84/suppl/C](https://www.sciencedirect.com/bookseries/international-geophysics/vol/84/suppl/C), 2002.
- Menviel, L., Capron, E., Govin, A., Dutton, A., Tarasov, L., Abe-Ouchi, A., Drysdale, R. N., Gibbard, P. L., Gregoire, L., He, F., Ivanovic,
550 R. F., Kageyama, M., Kawamura, K., Landais, A., Otto-Bliesner, B. L., Oyabu, I., Tzedakis, P. C., Wolff, E., and Zhang, X.: The penulti-
mate deglaciation: protocol for Paleoclimate Modelling Intercomparison Project (PMIP) phase 4 transient numerical simulations between
140 and 127 ka, version 1.0, *Geoscientific Model Development*, 12, 3649–3685, <https://doi.org/10.5194/gmd-12-3649-2019>, 2019.

- Musiak, Z. and Quarles, B.: Three Body Dynamics and Its Applications to Exoplanets, Springer Cham, <https://doi.org/10.1007/978-3-319-58226-9>, 2017.
- 555 Oliveira, E. D. and Fernandez, J. H.: Global resolved energy balance with galactic cosmic rays (greb-gcr) theory: a new simplified climate model, *Revista Brasileira de Geografia Física*, 13, 842–854, <https://doi.org/https://doi.org/10.26848/rbgf.v13.2.p842-854>, 2020.
- Oliveira, E. D., Fernandez, J. H., Mendes, D., Constantino, M. H., and Gonçalves, W. A.: Validation of a simplified climate model adapted to simulate the effects of increased CO₂ concentration associated with the galactic cosmic rays theory, *Revista Brasileira de Geografia Física*, 12, 768–778, <https://doi.org/https://doi.org/10.26848/rbgf.v12.3.p768-778>, 2019.
- 560 Otto-Bliesner, B. L., Braconnot, P., Harrison, S. P., Lunt, D. J., Abe-Ouchi, A., Albani, S., Bartlein, P. J., Capron, E., Carlson, A. E., Dutton, A., Fischer, H., Goelzer, H., Govin, A., Haywood, A., Joos, F., LeGrande, A. N., Lipscomb, W. H., Lohmann, G., Mahowald, N., Nehrbass-Ahles, C., Pausata, F. S. R., Peterschmitt, J.-Y., Phipps, S. J., Renssen, H., and Zhang, Q.: The PMIP4 contribution to CMIP6 – Part 2: Two interglacials, scientific objective and experimental design for Holocene and Last Interglacial simulations, *Geoscientific Model Development*, 10, 3979–4003, <https://doi.org/10.5194/gmd-10-3979-2017>, 2017.
- 565 Puetz, S. J., Prokoph, A., and Borchardt, G.: Evaluating alternatives to the Milankovitch theory, *Journal of Statistical Planning and Inference*, 170, 158–165, <https://doi.org/https://doi.org/10.1016/j.jspi.2015.10.006>, 2016.
- Yang, X.-S.: Chapter 28 - Mathematical Modeling, in: *Engineering Mathematics with Examples and Applications*, edited by Yang, X.-S., pp. 325–340, Academic Press, <https://doi.org/https://doi.org/10.1016/B978-0-12-809730-4.00037-9>, 2017.